EXPERIMENTAL AND NUMERICAL INVESTIGATION OF VOLTAGE DROP IN ANODE ASSEMBLIES

Ebrahim Jeddi[1], Daniel Marceau[1], Laszlo I. Kiss[1], Lyne St-Georges[1], Denis Laroche[2], Lyès Hacini[2]

[1]University Research Centre on Aluminium (CURAL) - Aluminium Research Centre (REGAL) - University of Québec at Chicoutimi; 555, Boul. de l'Université, Chicoutimi (Québec), Canada, G7H 2B1

[2]Rio Tinto Alcan (Arvida Research and Development Center); P.O. Box 1250, Jonquière (Québec), Canada, G7S 4K8

Keywords: Aluminum, Electrolysis, Modeling and Simulation, Anode Assembly, Finite Element, Voltage Drop

Abstract

Improving the Hall-Héroult process through reducing voltage drop in the anode assembly is one of the most challenging subjects for the primary aluminum production industry. In this paper, a fully coupled Thermo-Electro-Mechanical (TEM) model of a half carbon block submodel extracted from a full hexapod anode assembly is proposed in order to achieve a better understanding of its multi-physical behavior. This fully parametric Finite Element (FE) model was developed using APDL™ (ANSYS® Parametric Design Language) and was solved using a FESh++ TEM application. Special attention was paid to the good prediction of the contact conditions at the cast iron to carbon interface. First, the model was calibrated using experimental measurements realized by ARDC at Rio Tinto Alcan, and then used to investigate the phenomena taking place in the stub hole region with a focus on the contact at the cast iron to carbon interface.

Introduction

Today's aluminum industry is the subject of an international competition, which is forcing producers to reduce their production costs and pollutive emissions. Aluminum is extracted from alumina (Al_2O_3) using an electrolysis process called the Hall-Héroult process. The electric current used for this process is 150 to 500 kA depending on the technology. Theoretically, 6.0 MWh is needed to produce one metric ton of aluminum, while this value in practice is between 12.5 and 16.0 MWh demonstrating that there are opportunities to reduce the expenditure of energy. The target value by 2020 is 11 MWh/t as per Marceau *et al.* [1].

Voltage drop is used as the main index in evaluating the performance of the reduction cell or its main parts such as the anode assembly. The reason is the direct impact of the voltage drop on their efficiency, which is considerable in the long term. Fabrication of the anode assembly requires connecting and fixing its two main parts: the superior part and the carbon block(s). This is done through the rodding process in which special holes, called stub holes, are created in the carbon blocks. As the name implies, these holes are created to place stubs, which are, in turn, components of the superior part. Liquid cast iron is poured in the stub holes to fill the empty space; the result after solidification is a fairly good connection between steel stub and an air gap interface between cast iron and carbon. This initial air gap imposes electrical and thermal contact resistance against the electric current. Up to 25% of the anodic voltage drop is attributed to steel/cast iron/carbon interfaces [2]. Given this, to lower the anode voltage drop and, consequently, to lower production costs, a comprehensive study of the anode assembly, particularly its TEM behavior at interfaces as well as change in mechanical behavior of the materials during the process is needed.

TEM Problem

A reduction cell deals with many physical phenomena: thermal, chemical, electrical and mechanical are the most important ones in the aluminum production process [3]. These phenomena are not independent of each other, and they are especially significantly coupled at the cast iron/carbon interface. This interface will be referred to as **the interface** henceforth.

In aluminum smelting, an intensive electric current is applied through the busbar on top of the anode assembly. The electric current loses its potential during its path from anode to cathode mainly in two ways: material resistivity and contact resistance. The former is generally a function of temperature, which changes from one material composition to another. However, the potential for substantially decreasing this resistance is not much since it is the nature of the materials to impose resistance against the electric current and generate heat. This phenomenon is referred to in the technical literature as the Joule effect. The latter, which is a function of temperature and pressure, can be influencing if not controlled properly. However, its highly nonlinear TEM nature makes it difficult to easily understand its impact on the total efficiency of the anode assembly. This was the reason behind a long history of research on the contact resistance, which resulted in several mathematical and numerical models [for details see 4].

The heat generated by the Joule effect causes thermal expansion. The expansion first fills up the initial gap at the interface once the anode assembly is set to operation. With an increasing temperature after contact establishment, the thermal expansion causes contact pressure, which, on the one hand, can be, detrimental if excessive. This is due to the low tensile strength of the anode carbon. On the other hand, increasing temperature and contact pressure lowers the contact resistance at the interface, and consequently, more current is conducted through. With a higher current density, the heat generation by the Joule effect increases, and this cycle repeats until it reaches an approximate steady state condition. Apart from expansion, a change in the TEM properties can change the behavior of the anode assembly e.g. with temperature-dependent mechanical properties, the stiffness of the solid components will vary with a change in the thermal flow since it causes a change in temperature. This is not only true for the materials, but also for the interface too.

Previous Work

Although previous work on the anode assembly can be classified into two main categories (experimental and/or *in situ*, numerical) the focus in this paper will be the numerical models. The first efforts to build a model to solve the problems of the reduction cells and the aluminum production process go back to the 1980s [see 5]. In addition, there have been several analyses carried out

recently to reduce the voltage drop in the anode assembly through different approaches; nevertheless, most of them could not simulate the anode system and reduction process adequately due to many geometrical simplifications and lack of consideration accorded to all thermal, electrical and mechanical phenomena simultaneously.

Richard was the first to develop an ANSYS based TEM anode stub hole model [6,7]. Unfortunately the ANSYS version available at the time did not support TEM contact elements and thus prevented the development of a fully coupled model. Following Richard's initial effort, Goulet developed a fully coupled TEM model based on the in-house object-oriented FE code FESh++[8, 9]. FESh++ supports the implementation of complex material constitutive laws, for instance for carbon based materials; therefore, it is extremely useful to carry out advanced research work [see 10]. Kandev and Fortin [11] presented their simplified Thermo-Electrical (TE) in 2009. A more simplified TE model was presented by Li *et al.* [12]. In the same year, Fortin *et al.* [13] presented a TEM model of a tripod anode assembly to evaluate the influence of the stub degradation on the anodic voltage drop. Also, Richard *et al.* [6] tried to investigate the impact of number of flutes on the voltage drop using their TEM model. Dupuis [7] built an ANSYS TEM stub hole design tool in 2010. Most recent works belong to Beier [14] in 2011, Fortin *et al.* [15] in 2012, and Jeddi *et al.* in 2012 [4, 16]. All of the recent models were TEM.

Experimental Model

To date, almost all of the numerical models used *in situ* measurements or experiments simulating smelting conditions. However, the authors have outlined a new approach to simplifying the complications of the thermal gradient and the Joule effect thus creating more stable conditions in which to study the phenomena taking place at the interface. The main purpose of the experiments was to provide authentic information for the numerical model, and also to investigate potential distribution and contact status at different temperatures. The tests were designed and executed by ARDC. Figure 1 shows the electrical contact furnace used to carry out the experiments.

Figure 1- Electrical Contact Furnace

Specific positions in the experimental model components were selected where several probes were inserted to capture electrical potential. The positions of the sensors used in the figures of results in this paper are illustrated in Figure 2. The strategy was to record electrical potential at temperatures from 400°C to 950°C in steps of 100°C except for the last step, which was an increment of 50°C. A special support was designed to which the experimental

model was fixed before performing the tests. Once placed in the furnace, the model was given enough time to reach a uniform temperature in each step, and then, an electric current of 1kA was conducted from the top of the stub. Potential readings by the voltage probes were recorded after approximately 3 minutes to make sure that the current flow was in a steady state condition.
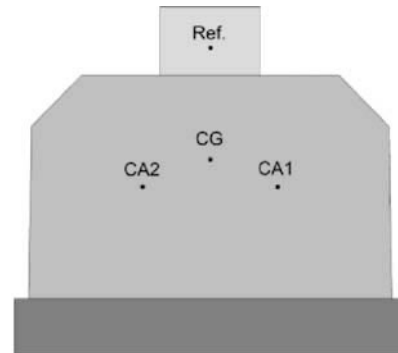

Figure 2-Voltage probe configuration

FE Model

Geometry and features

A full anode assembly model was first developed using APDL 12.0. The full model is the most realistic one in terms of geometrical modeling yet presented. It also offers features such as: number of flutes, shape of flutes (flute design), malpositioning of stub into stub hole, pancake formation, carbon consumption, and capability to generate submodels [for details see 4]. To study the TEM phenomena taking place in the stub hole region, a model called half block model was extracted from the full model. The half block model, which is depicted in Figure 3, was fixed on a support to perfectly represent its experimental setup.
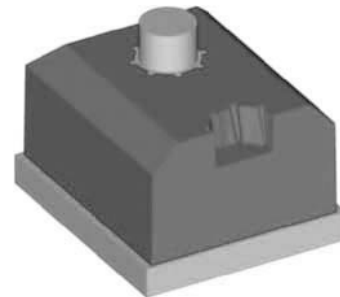

Figure 3-Half block model

Material properties

Carbon was supposed linear elastic. Electrical resistance of the carbon was assumed to be orthotropic as per Wilkening and Côté [17]. Support was considered an isotropic thermo-elastic material. The stubs and the cast iron connectors were considered isotropic thermo-electro-elastic materials. Experimental results obtained at CURAL were used for the thermal expansion of steel and cast iron with respect to temperature. Most of the material properties used in this model are confidential, and therefore cannot be published owing to the non-disclosure agreement with ARDC/RTA.

Contact

Very high electrical contact resistance was applied to the bottom the stub and the cast iron connector. Good contact between the stub and the cast iron connector was assumed. The support was set to have a Thermal Multi Points Constraint (TMPC) with carbon. The contact properties applied to the interface were the properties obtained through the experiments by Rouleau [18].

Since transition from non-contact to contact condition or vice versa can cause oscillation, and consequently convergence problems, a Hermitian function was used to smoothen this transition [4].

Boundary conditions (BCs) and mesh

Constant temperatures (400°C-950°C), according to the steps of the experiments, were applied to the whole model in each step. A current density corresponding to 1 kA current was applied to the top of the stub. The bottom of the carbon block was set to zero volts. The stub was fixed for the horizontal movements (x-y directions) at the nodes on the edge of the top surface; however it was left free to move along its height (z direction). Also, the support was fixed at its bottom surface. Finally, the weight of the entire model was considered to be the body load, which provides conditions required to establish contact owing to lack of internal forces generated. Table 1 summarizes the mesh composition.

Table 1: Mesh composition

Component	Element Type	Number of Elements
Solid	Linear Hexahedral, 3D Coupled Field Solid	57123
Contact	Linear Shell	10685
BCs	Linear Shell	6953
Total	**Nodes: 65479**	**Elements: 63239**

Solution strategy and load steps

The Newton-Raphson solution technique was employed to solve the fully coupled TEM problem. At each iteration, thermal, electrical and mechanical problems were solved simultaneously, and subsequently the global equilibrium of the governing equations was updated with the updated values of each field. Since this method applies the impact of all of fields at the same time in each iteration it is faster than solving the weakly coupled problem. Contact problems are delicate to solve due to their highly nonlinear nature. Numerosity of contact (numerous surfaces in contact) in one single model adds to its complexity. Since the model was TEM and included contact in several parts, to avoid any problem causing divergence loads were applied in 3 steps as shown in Figure 4.
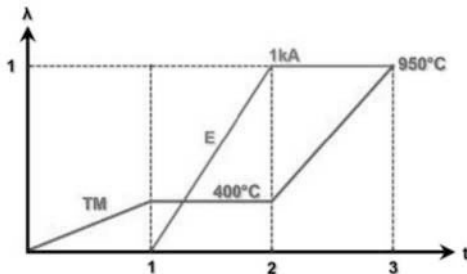

Figure 4-Load steps

Step 1 consists of one single substep; Step 2 consists of 2 substeps and Step 3 consists of 6 substeps (equivalent to the number of time intervals to reach 950°C from 400°C). In the aforementioned figure, t is the axis of steps and λ is the axis of load application progress where at 1 loads are applied in full

Initial air gap

Numerical modeling of the anode assembly began years ago; nonetheless, not much research work has been done on the prediction of the initial air gap. Linear functions, which calculate the radial thermal contraction of the stub and cast iron, have been widely used in researches. These equations, proposed by Richard [see 6], are shown in Equations (1) and (2) where g is the air gap size; z, the vertical axis perpendicular to the carbon block bottom surface; α, the secant Coefficient of Thermal Expansion (CTE); T_{ph}, the effective stub temperature at cast iron solidification; T_0, the ambient temperature; t, the thickness of cast iron, and T_s is the solidification temperature of cast iron. Equation (1) calculates the radial contraction of the stub. Equation (2) calculates the total air gap size through adding the radial contraction of the cast iron to the value obtained from Equation (1). The shortcoming of these equations is that the lateral gap of the flutes is not considered. To cope with this problem, the authors used Equation (2) with $\gamma = 0$ and applied half of the resultant value on each side.

$$\gamma = R_{stub}\alpha_{steel}(T_{ph} - T_0) \tag{1}$$

$$g(z) = \gamma + (t(z) - \gamma)\alpha_{castiron}(T_s - T_0) \tag{2}$$

Employing the aforementioned equations to calculate the initial air gap requires the determination of three air gap zones: cylindrical portion, tip of the flutes and side of the flutes. Furthermore, since the thickness of the cast iron changes from top to bottom, the magnitude of the air gap varies linearly along its height. Unlike previous work that considered uniform gap for each zone, in this work, variable air gap profile was considered for each zone according to the explanation above.

Calibration

Sound calibration is an inescapable part of a reliable simulation process. Measurements obtained from the experimental setup were used to calibrate the half block model. A series of parameters were taken into account in a specific order to calibrate the model. The start model using the initial values for parameters is called the **Base model** (or simply "Base" on the charts). After each series of simulations on a single parameter, a decision was made to choose the best fitting value of that parameter and the remainder of the simulations (in the list) were executed with the updated model. First, the model was calibrated for the numerical parameters. This part of the calibration is to ascertain that the model converges successfully. Then, the model was calibrated for the physical parameters such as frictional coefficient, air gap distribution (T_{ph} and lateral gap of flutes) and electrical resistance of carbon (horizontal and vertical).

Since the calibration of the air gap distribution revealed important information on how contact establishes and develops, only calibration of T_{ph} and lateral gap of flutes are elaborated here. The details of the entire calibration process can be found in [4].

Results and Discussion

Virtual sensors were implemented in the numerical model in exactly the same positions that the voltage probes have been inserted in the experimental model to correctly reflect the same potential readings [see Figure 2]. Several combinations of sensors were selected to evaluate the potential loss in the model. However, only a few of them are presented here. Note that CA in the figures represents an average of CA1 and CA2.

Figure 5 demonstrates the results of the simulations to adjust T_{ph}. As explained previously in the **Initial air gap** section, T_{ph} is the effective stub temperature at cast iron solidification. Considering the rodding process and complex geometry of the cast iron connector, it is concluded that the poured cast iron does not solidify at once. In addition, the solidification of the cast iron depends on many conditions, such as the temperature of the liquid cast iron at the time of casting, temperature distribution of the carbon block, heat transfer properties of the materials etc. It is clear that the accurate measurement of T_{ph} will be extremely difficult. On the other hand, of all of the parameters required to calculate the initial air gap magnitude using Equations (1) and (2), T_{ph} is the only unknown one. The remainder of the parameters can be measured as they have been in this work. Therefore, T_{ph} is used as a calibration parameter. The only point that should be noticed here is the fact that T_{ph} does not contribute to the calculation of the lateral gap size. Thus, one more series of simulations is required to adjust the lateral gap of the flutes as well.
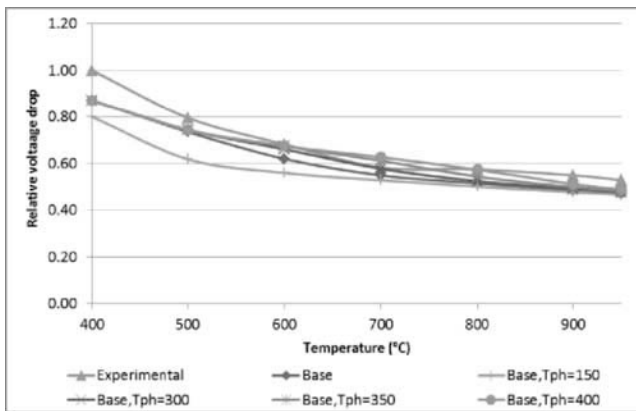

Figure 5- Calibration of the T_{ph} (CA-Ref)

Respecting the confidentiality agreement with the industrial partner, the results of the experimental tests have been scaled to [0,1], and the other simulations have been scaled relative to the experimental results.

Figure 5 compares the results of 5 series of simulations to the experimental results. Prior to T_{ph}, numerical parameters and some physical parameters have been adjusted. However, the discussion about them is beyond the scope of this paper. The initial (start) value for T_{ph} was 250ºC. The blue curve with rhombus markers represents the updated base model. The other simulation curves represent the results of the simulation with a different T_{ph}.

The first thing that can be noted from the figure is that with an increasing T_{ph} generally the voltage drop increases. The reason is that a higher T_{ph} results in a larger gap at the cylindrical portion and tip of the flutes. However, this is not true for the temperatures above 250ºC when it comes to the initial parts of the curve, especiallyat 400ºC-500ºC. It was conceived that contact is not controlled by these two zones of the interface, and the only remaining zone was the sides of the flutes.

The next series of simulations corroborated this expectation. These results, which are illustrated in Figure 6, showed that the contact on the sides of the flutes has an essential impact on the total contact condition, and thus voltage drop at lower temperatures. The lateral gap size for the base model was calculated using Equation (2) according to the section **Initial air gap**. The lateral gap was increased until a good agreement between the numerical curve and the experimental one was achieved. It was concluded that the size of the gap on the sides of the flutes must be 20% larger than that obtained from the linear distribution.
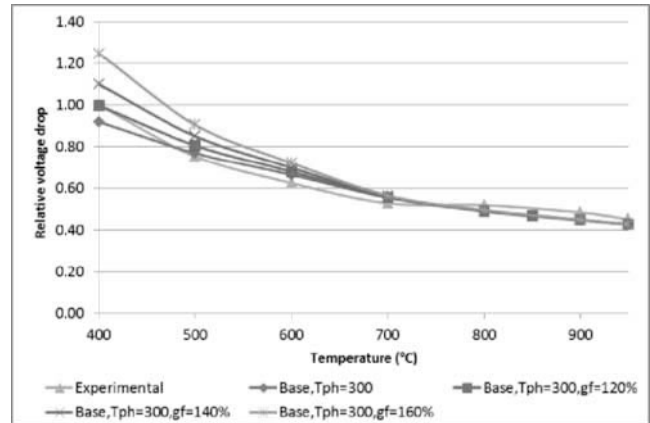

Figure 6- Calibration of the lateral gap of flutes (CG-Ref)

Moreover, after 700ºC, all of the simulations give approximately the same value for the voltage drop. It is clear from Figure 6 that the impact of the sides of the flutes diminishes gradually until 700ºC that the contact established at the other zones (cylindrical portion and tip of the flutes) becomes completely dominant.

All of the explanations can be seen in the next three figures. Figure 7 is the contour plot of the contact condition at the interface at 400ºC. The legend presented for the contact status plots in Figure 7 is mainly used as an indication of the quality of contact. The range between 0 and 1 is assumed to be a no contact condition. This range has been color-coded with different shades of blue. Approaching 1 and exceeding is interpreted as establishing contact, while contact in the range of 1 to 2 is considered sliding contact. It is assumed that with exceeding 2 contact turns to sticking due to enough contact pressure, which is better in terms of quality.

From Figure 7 it is clear that contact establishes on the sides of the flutes at the lower part of the interface. This is in accordance with what can be concluded from Figure 6. Newly implemented statistical features in FESh++ generated interesting data such as the percentage of the contact area. It was seen that at 400ºC only 12% of the entire interface surface contributed to contact.
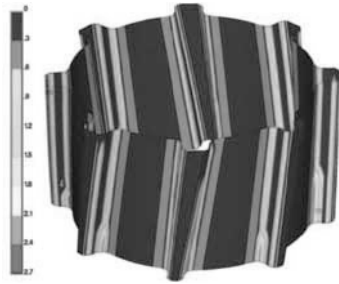
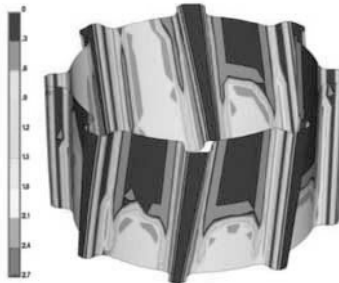Figure 7- Contact condition at the cast iron to carbon interface at 400°C (contact area: 12%)

Figure 8- Contact condition at the cast iron to carbon interface at 700°C (contact area: 42%)
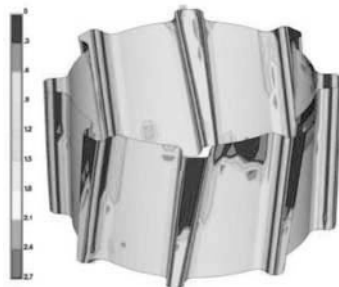

Figure 9- Contact condition at the cast iron to carbon interface at 950°C (contact area: 70%)

With increasing the temperature to 700°C, contact propagates to higher parts, and is also established on the cylindrical portion as well as on the tip of the flutes. This development, which can be seen in Figure 8 with 42% contact area ratio, is dominant enough to diminish the influence of the flue sides on the contact condition. Such a contribution becomes much higher at 950°C, where 70% of the entire interface contributes to contact. However, it is unlikely that, in the actual smelting conditions, the stub hole region would reach such temperatures. There has been no accurate measurement published thus far about the temperature of the stub hole region under real operating conditions; however, the effective temperature is expected to be around 700°C ±100°C. That being said, Figure 8 represents a good approximation of the contact status even though the thermal gradient from bath or convection on all of the surfaces of the anode assembly was not considered. It should be borne in mind that the contact area ratios mentioned here are not real contact areas that effectively contribute to decreasing contact resistance. More simulations with

the half anode assembly or full anode assembly model will reveal such information.

Figure 10 illustrates how the contact area ratio and contact resistance at the interface evolve with respect to temperature. It shows that from 600°C to 700°C the contact area ratio rises rapidly. Even though a great improvement in terms of contact area ratio occurs, contact resistance does not decrease accordingly. It indicates that the contact area ratio is not the only parameter to be taken into account in evaluating the quality of contact. It is expected that the current density play an important role in such evaluation.
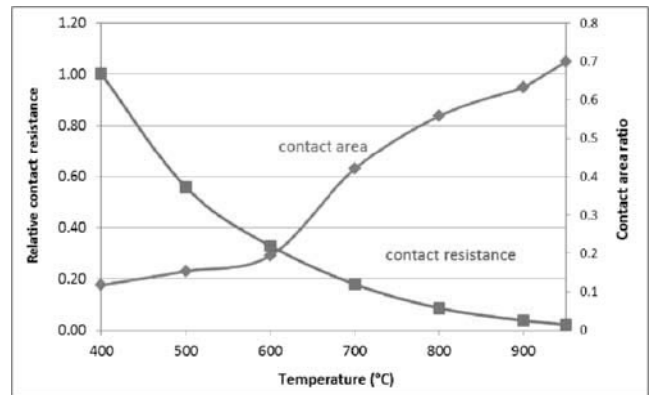

Figure 10- Evolution of contact status

Carbon used in the anode assemblies of different designs has approximately 30 MPa and 5 MPa of ultimate compressive and tensile strength respectively. It is clear that with a fairly low tensile strength, carbon is prone to fail or damage under tension. That being said, the first principal stress (S1) becomes an important criterion to be checked for any design or optimization recommendations. In Figure 11, which demonstrates the first principal stress distribution at 700°C and 950°C, the green in the contour plots represents a stress between 4 to 15 MPa; thus, considering an ultimate strength of 5MPa, carbon failure is possible even at 700°C. Since linear elastic material was used for carbon, the model cannot predict possible failure or damage. However, it is thought that actual carbon material could tolerate localized high stress through local material failure, which does not necessarily result in a crack and follow-up propagation. In some cases, though, cracks were witnessed.

The maximal stress at 950°C exceeded 59 MPa on the surfaces of the flute slots in the stub hole which can be seen in red. In spite of the very high stress on some parts of the flute slots' surface, the dominant stress range in the material remained 4MPa-15 MPa (green). The consequence of such high stress in the material cannot be easily determined unless a more developed constitutive law is used for carbon.
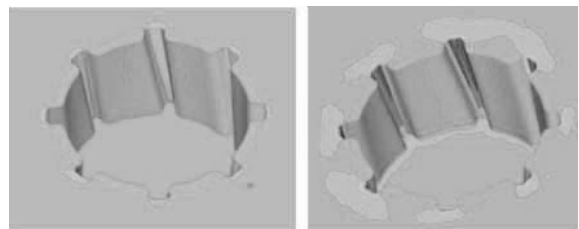

Figure 11- 1st principal stress- 700°C (left) & 950°C (right)

Conclusions

Simulation during the calibration process of the air gap distribution at the cast iron to carbon interface revealed that contact establishes on the sides of the flutes at lower temperatures (400°C-500°C), and then propagates to the cylindrical portion and the tip of the flutes. At 700°C and higher, the contribution of the flute sides to contact diminishes.

Assuming that in operation the temperature in the stub hole lies somewhere in 700°C ±100°C range where the total contact area may not even reach 50% of the total area at the cast iron to carbon interface, finding solutions to increase the contact area through geometrical (design) optimization or correcting the composition of the material in order to obtain better contact would be a challenging but worthwhile goal. However, the importance of an in-depth investigation of the quality of contact is also crucial. It was demonstrated that contact area increase may not improve the quality of contact, thus decreases the contact resistance. Finding a way such as defining a parameter or an index to evaluate the effectiveness of contact would be a good idea.

Employing a realistic constitutive law for carbon is still one of the most important needs in this domain of research. Lack of such implementation makes it difficult to easily draw conclusions about the anode carbon's susceptibility to failure under stress.

References

[1] D. Marceau, S. Pilote, M. Désilets, J-F Bilodeau, L. Hacini, Y. Caratini, Advanced numerical simulation of the Thermo-Electro-Chemo-Mechanical behaviour of Hall-Héroult cells under electrical preheating, Proc. of TMS Light Metals, 2011, pp. 1041-1046

[2] R.W. Peterson, Studies of stub to carbon voltage, Proc. of TMS Light Metals, 1978, pp. 367-378

[3] D. Richard, M. Fafard, R. Lacroix, P. Cléry, Y. Maltais, Aluminum reduction cell anode stub hole design using weakly coupled thermo-electro-mechanical finite element models finite element models, J. Finite Elem. Anal. Des. 37 (2001) pp. 287-304

[4] E. Jeddi, Numerical study of anodic voltage drop in the Hall-Héroult cells by finite element method, Master's thesis, UQAC, Canada, 2012

[5] http://www.genisim.com/download/epfl2004.htm

[6] D. Richard, P. Goulet, O. Trempe, M. Dupuis and M. Fafard, Challenges in stub hole optimisation of cast iron rodded anodes, Proc. of TMS Light Metals, 2009, pp. 1067-1072

[7]M. Dupuis, Development and application of an ANSYS based Thermo-Electro-Mechanical anode stub hole design tool, TMS Light Metals 2010, pp. 433-438

[8] P. Goulet, *Modélisation du Comportement Thermo-Électro-Mécanique des Interfaces de Contact d'une Cuve de Hall-Héroult*, Ph. D. Thesis, Laval University, Quebec, Canada (2004)

[9][ ] H. Fortin, M. Fafard, N. Kandev, and P. Goulet, FEM Analysis of Voltage Drop in the Anode Assembly, Proc. TMS Light Metals 2009, pp. 1055-1060

[10] D. Marceau, P. Goulet, D. Richard, M. Fafard, FESh++, *Une Nouvelle Approche Orientée Objet pour la Simulation par Éléments Finis des Problèmes Multiphysiques*, $7^{ème}$ *Colloque National en Calcul des Structures*, Giens, France, 2005, pp. 303-308

[11]N. Kandev, H. Fortin, Electrical losses in the stub-anode connection: computer modeling and laboratory characterization, TMS Light Metals, 2009, pp. 1061-1066

[12] W. Li, J. Zhou, Y. Zhou, Numerical analysis of the anode voltage drop of a reduction cell, Proc. of TMS Light Metals, 2009, pp. 1169-1171

[13][ ] H. Fortin, N. Kandev and M. Fafard, FEM analysis of voltage drop in the anode connector induced by steel stub diameter reduction, Finite Elem. Anal. Des. 52 (2012) pp. 71-82

[14] S. Beier, J.J.J. Chen, H. Fortin and M. Fafard, FEM analysis of the anode connection in aluminum reduction cells, Proc. of TMS Light Metals, 2011, pp. 979-984

[15] H. Fortin, N. Kandev and M. Fafard, FEM analysis of voltage drop in the anode connector induced by steel stub diameter reduction, Finite Elem. Anal. Des. 52 (2012) pp. 71-82

[16]E. Jeddi, D. Marceau, L. I. Kiss, L. St-Georges, D. Laroche, L. Hacini, Thermo-Electro-Mechanical investigation of voltage drop in anode assembly using finite element method, 10th Congress on Computational Mechanics, 2012

[17] S. Wilkening and J. Côté, Problem of the stub-anode connection, Proc. of TMS Light Metals, 2007, pp.865-873

[18]M. Rouleau, Caractérisation thermo-électro-mécanique des interfaces fonte-acier-carbone dans une cuve d'électrolyse, Master's thesis, UQAC, 2007